Nanoscale Res Lett (2010) 5:863–867
DOI 10.1007/s11671-010-9576-3

NANO EXPRESS

A New Extension of Cauchy–Born Rule for Monolayer Crystal Films

Sheng Lu · Chongdu Cho

Received: 23 February 2010 / Accepted: 5 March 2010 / Published online: 23 March 2010

Abstract By combining with the physical concept of inscribed surface, the standard Cauchy–Born rule (CBR) is straightly extended to have a rigorous and accurate atomistic continuum theory for the monolayer crystal films. Resorting to using Tersoff–Brenner potential, the present theory to graphite sheet and single-walled carbon nanotubes (SWCNTs) is applied to evaluate the mechanical properties. The results are validated by the comparison with previously reported studies.

Keywords Carbon nanotubes · Cauchy–Born rule · Monolayer crystalline film · Inscribed surface · Mechanical properties

Introduction

Based on atomistic simulations, a series of values of mechanical properties of CNTs are given and agreed qualitatively with experimental studies, but such methods quickly become computationally extremely demanding as the number of atoms increases. In other words, there exists a rigorous limitation on atomistic simulation by its time and length scales. So, a direct link between the continuum analysis and atomistic simulation is needed to investigate the mechanical properties of CNTs more effectively. In general, the so-called CBR [1, 2] is viewed as the fundamental assumption for linkage between the deformation descriptions of crystal configurations and the continuum theories of crystal mechanics. Without considerations of diffusions, phase transitions, lattice defects, slips, or other non-homogeneities, it is quite suitable for the space-filling materials. In a space-filling material, the crystal deformation is homogenous and continuous at the atomic scale, and the lattice vector and its tangent are coincident. Thus, CBR is widely accepted as the form of $\mathbf{a} = \mathbf{F}\cdot\mathbf{A}$, where $\mathbf{F}$ denotes a two-point deformation gradient tensor, $\mathbf{A}$ and $\mathbf{a}$ denote one lattice vector on the respective undeformed and deformed crystals.

However, the standard CBR fails to extend directly to the case of monolayer crystal films. In short, if the monolayer crystal film is treated as a surface, the deformation gradient $\mathbf{F}$ maps the tangent space of the surface and the lattice vectors are regarded as chords of the surface. Obviously, the finite length lattice vector does not fall into the tangent space of infinitesimal material vectors, so the deformation gradient $\mathbf{F}$ cannot give an accurate description of relationship between the undeformed and the deformed lattice vectors.

To generalize the standard CBR in the monolayer crystal films, two main type modifications are developed until now. In the study of finite crystal elasticity for curved single layer lattices, Arroyo and Belytschko [3, 4] developed the exponential CBR. First, the undeformed lattice vector $\mathbf{A}$ is mapped into the tangent space by the exponential inverse mapping to get an undeformed finite line element. After the deformation calculations of finite line element on the tangent space, the deformed finite line element on the tangent space is pulled back to the deformed surface by the exponential mapping to determine the deformed lattice vector $\mathbf{a}$. In practice, it requires the knowledge of the geodesic curves of the surface. That means much computational cost is needed to pay to solve a set of non-linear partial differential

S. Lu · C. Cho (✉)
Department of Mechanical Engineering, Inha University, Inchon 402-751, South Korea
e-mail: cdcho@inha.ac.kr

S. Lu
e-mail: slu@inha.ac.kr

equations. Besides, on the deformation gradients in atomistic continuum modeling, Sunyk and Steinmann took into account the second quadratic term in the Taylor's series expansion of the deformation field [5]. Then, Guo et al. [6] and Wang et al. [7] performed the higher order CBR for predicating the mechanical properties of SWCNTs. For the monolayer films, they illuminated that higher order term of the deformation gradient can pull the tangent vector close to the deformed manifold. Sometimes, this method has to be in the face of convergence problem. Both of two modified CBRs mentioned in the above are approximate methods from mathematics. However, based on the physical concept of inscribed surface, the present study discovered that the standard CBR can be extended straightly to describe monolayer crystal films accurately.

New Extension of CBR

As shown in Fig. 1, one atomic chain ABCDE including five atoms marked by solid circles is deformed to one equilateral pentagon from a line. The sides of equilateral pentagon are tangent to its inscribed circle C_2 at five open circles *m*, *n*, *o*, *p*, *q*. The circumcircle of this equilateral pentagon is denoted by C_1. At the straight line state of Fig. 1a, the circumcircle C_1 and the inscribed circle C_2 recovery back to straight atomic chain. If one-dimensional deformation along this line is considered, the atomic chain can be treated as the space-filling materials. The standard CBR can be introduced directly due to the lattice vector and its tangent coincide particularly well to each other. However, at the equilateral pentagon state of Fig. 1b, this atomic chain is always viewed as the curve C_1 generally owing to the position of atoms. If the standard CBR is applied to the atomic curve C_1, it means the deformation of the bond AB is described by tangent behavior along the direction of AK. So errors will be inevitably introduced.

Interestingly, the chord AB of circumcircle C_1 exactly is the tangent of the inscribed circle C_2 at any time of deforming. That is to say, the deformation gradient of the lattice vector AB maps the tangent space of the inscribed circle C_2 at tangent point *m*. In other words, the variation of the bond (the chord of the circumcircle C_1) can be investigated by the deformation gradient (the tangents) of the inscribed circle C_2 at the tangent point.

Generally, inscribed curves for one atomic chain are not unique due to the positions of tangent points as shown in Fig. 1c. That means different tangent points offer different inscribed curves. In the practical calculations, the representative cell should be introduced. Due to the axisymmetry of every two representative cells, this tangent point should be selected as the middle point of each bond. By applying this idea to the three-dimensional structures of SWCNTs as shown in Fig. 2, monolayer crystal films can use the tangent space of their inscribed surface to describe the deformations of their bonds [8]. Furthermore, as indicated by Cousins [9], Tadmor et al. [10], and Zhang et al. [11], the inner equilibrium of the representative cell in the non-centrosymmetric structure as SWCNTs cannot be guaranteed by CBR. With introducing the inner shift vector $\boldsymbol{\lambda}$, the lattice vector is expressed as:

$$\mathbf{a} = \mathbf{F}(\mathrm{A}/2, \boldsymbol{\lambda}) \cdot (\mathrm{A} + \boldsymbol{\lambda}), \tag{1}$$

where **A** and **a** denote one lattice vector in the undeformed and deformed crystals, respectively; the deformation gradient based on the inscribed surface of $\mathbf{F}(\mathbf{A}/2,\boldsymbol{\lambda})$ is function of the position of middle point of undeformed lattice vector **A** as well as the inner shift vector $\boldsymbol{\lambda}$. So the method of using the deformation gradient of the tangent point on the inscribed surface to describe the deformation of whole lattice vector of single-layer crystal film is developed. This extension is named the inscribed CBR due to main reference is inscribed surface.

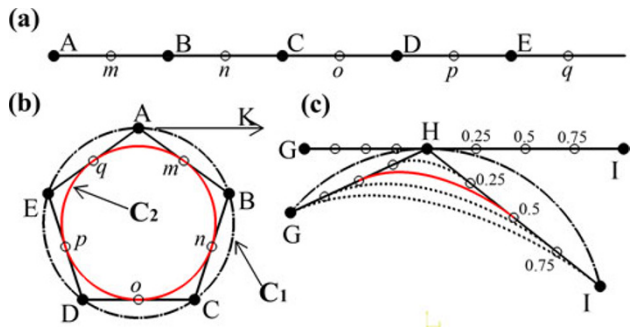

Fig. 1 Illustration of an atomic chain deformed in two dimensional spaces

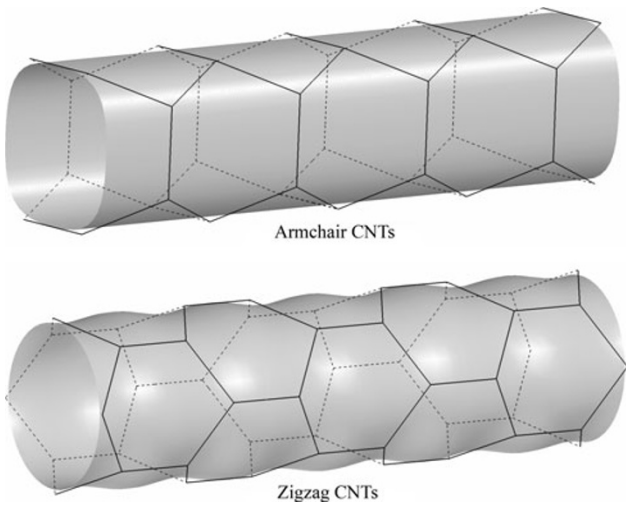

Fig. 2 The inscribed surface models for each type SWCNT (the inner shift between two sub-lattices is not considered in this figure)

Table 1 The extensions of CBR for different types of materials

Monolayer crystal film		Space-filling material	
Non-centrosymmetric	Centrosymmetric	Non-centrosymmetric	Centrosymmetric
$\mathbf{a} = \mathbf{F}(\mathbf{A}/2, \boldsymbol{\lambda}) \cdot (\mathbf{A} + \boldsymbol{\lambda})$	$\mathbf{a} = \mathbf{F}(\mathbf{A}/2) \cdot \mathbf{A}$	$\mathbf{a} = \mathbf{F} \cdot (\mathbf{A} + \boldsymbol{\lambda})$	$\mathbf{a} = \mathbf{F} \cdot \mathbf{A}$

All the deformation gradients in monolayer crystal film are based on inscribed surface

By the way, for the crystal film with centrosymmetric structure, the inner shift $\boldsymbol{\lambda}$ in Eq. 1 disappears. Moreover, for the space-filling materials in homogenous deformations, inscribed surface and atomic surface are superposed, so Eq. 1 is rewritten back to the standard CBR. To be brief, those modifications are summarized as shown in Table 1.

Applications to Graphite Sheets and SWCNTs

SWCNTs are viewed as results of rolling up different size graphite sheets along the different directions. Figure 3 shows the cross section of armchair CNT (2, 2) in the whole process of rolling up deformation. In the undeformed state, the black width lines *PQ* and *QR* along the axis $\mathbf{X}_2$ denote the representative cell *A* and *B*, respectively. In the deformed state, three dashed lines from the outer to the inner (in red, black, and blue) denote the configurations of the atomic surface, the C–C bond, and the inscribed surface without considering the shift vector $\boldsymbol{\lambda}$, respectively. Following the same logic, three solid lines from the outer to the inner show the configurations of the atomic surface, the C–C bond, and the inscribed surface with incorporating the shift vector $\boldsymbol{\lambda}$, respectively.

From the outer dashed line (the atomic surface without considering the inner shift) to the outer solid line (the atomic surface with considering the inner shift), there is no change except that the radius of circle becomes a little larger. This is so called the phenomenon of relaxation. However, by comparing with the inner dashed curve (the inscribed surface without considering the inner shift), the inner solid curve *pqr* (the inscribed surface with considering the inner shift) has obvious changes in shape to average the curvature distribution. From the view of energy, the curve with small curvature will be much steadier than with large curvature. So it is not difficult to say that the inner shift gives the deformation gradient a self-adjustment to uniformly distribute the energy. This adjustment of energy distribution of the inscribed surface can be comprehended as the physical origin of relaxation.

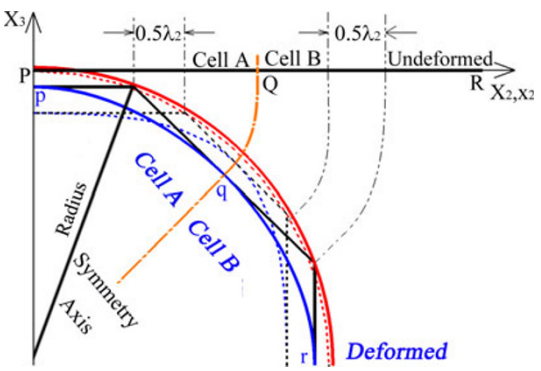

Fig. 3 The mapping of rolling up a graphite sheet to an armchair CNT

With the use of the geometric relationships in Fig. 3, the radius of atomic surface of armchair CNT r_a is obtained as:

$$r_a = \frac{4\sin(\frac{\pi}{m+n})}{\sqrt{a^2[5 + 4\cos(\frac{\pi}{m+n})] + (8\lambda_2^2 - 4a\lambda_2)[1 - \cos(\frac{\pi}{m+n})]}}. \tag{2}$$

By the same logic, the radius of atomic surface of zigzag CNT r_a is expressed as:

$$r_z = \frac{4\sin(\frac{\pi}{m+n})}{\sqrt{6a^2[1 + \cos(\frac{\pi}{m+n})] + 8\lambda_2^2[1 - \cos(\frac{\pi}{m+n})]}} \tag{3}$$

where a is the equilibrium bond length of graphite sheet, r_a and r_z denote the respective radii of armchair CNTs and zigzag CNTs. Obviously, the radii of SWCNTs depend on a pair of parameters (n,m) as well as the inner shift $\boldsymbol{\lambda}$.

Based on Brenner's interatomic potential [12, 13], the present study gives graphite sheet lattice constant of 0.145068 nm and equilibrium graphite sheet energy of −7.3756 eV per atom. The strain energies of bending are defined by assuming that the zero strain energy state corresponds to the equilibrium graphite sheet. By homogenizing this strain energy over its representative cell in the undeformed configuration leads to strain energy density of $W = W[\mathbf{F}_1,\mathbf{F}_2,\mathbf{F}_3,\boldsymbol{\lambda}]$, where subscripts 1, 2, and 3 means three C–C covalent bonds in one representative cell. By minimizing the strain energy of representative cell with respect to $\boldsymbol{\lambda}$, the inner shift vector is obtained by $\partial W/\partial\boldsymbol{\lambda}|_{\boldsymbol{\lambda}=\bar{\boldsymbol{\lambda}}} = 0$. Then, the radii of SWCNTs are determined by Eqs. 2 and 3. Compared with the undeformed circumference of $a\sqrt{3(n^2 + mn + m^2)}$ in the graphite sheet, in the rolling up of a graphite sheet to SWCNT, the strain in the circumferential direction is independent of the bending direction as shown in Fig. 4.

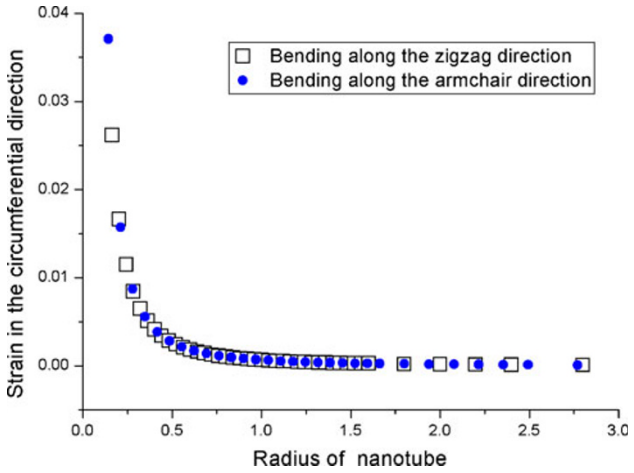

Fig. 4 The circumferential strains during the rolling up of graphite sheet to SWCNT versus the nanotube radius

The strain energies of bending are determined as shown in Fig. 5, which are in good agreement with results from molecular dynamics (MD) simulations [14]. With the same atomic surface curvature, bending along the zigzag direction has larger strain energy per atom than along the armchair direction. That is due to the inscribed surface of zigzag CNT has not only the same circumferential curvature deformation as armchair CNT (see Fig. 4) but also its own longitudinal curvature deformation (see Fig. 2). Meanwhile, by comparing with the curve $L\kappa^2/2 (L = 0.8\ \text{eV})$, the strain energy increase scales with κ^2 only at small bending curvature.

Then, the first Piola–Kirchhoff stress tensor **P** is derived by

$$\mathbf{P} = \sum_{i=1}^{3} \left[\frac{\partial W}{\partial \mathbf{F}_i} + \frac{\partial W}{\partial \lambda} \frac{\partial \lambda}{\partial \mathbf{F}_i} \right] \Bigg|_{\lambda = \bar{\lambda}} \tag{4}$$

and the modified tangent modulus tensors is expressed as

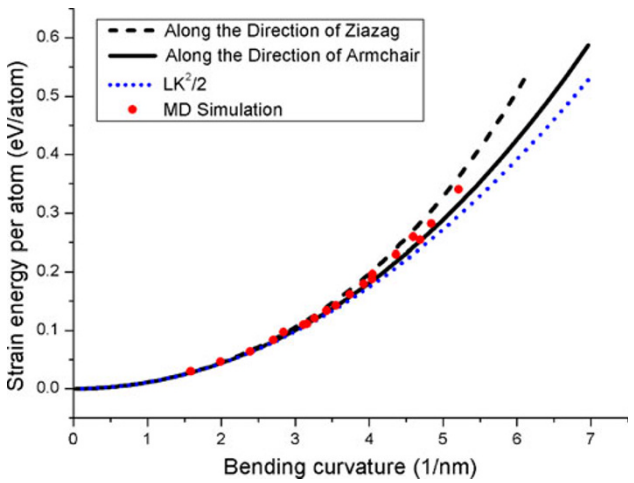

Fig. 5 The strain energy per atom during bending of graphite sheet versus the bending curvature

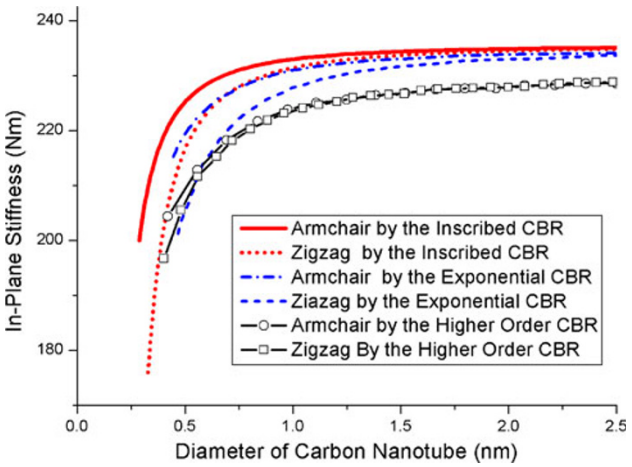

Fig. 6 In-Plane stiffness of SWCNT versus diameter of nanotube

$$\mathbf{Q} = \sum_{i,j=1}^{3} \left[\frac{\partial^2 W}{\partial \mathbf{F}_i \partial \mathbf{F}_j} - \frac{\partial^2 W}{\partial \mathbf{F}_i \partial \lambda} \cdot \left(\frac{\partial W^2}{\partial \lambda \partial \lambda} \right)^{-1} \cdot \frac{\partial W}{\partial \lambda \partial \mathbf{F}_j} \right] \Bigg|_{\lambda = \bar{\lambda}} \tag{5}$$

Based on Cartesian coordinates (x_1,x_2,x_3) as shown in Fig. 3, x_1 denotes the axial direction of a SWCNT, and x_2, x_3 locate on the cross section. For the simple tension along the axial direction x_1 of tube, Young's modulus is obtain as: $Yh = \mathbf{Q_{1111}} - (\mathbf{Q_{1122}})^2/\mathbf{Q_{2222}}$, where Y is Young's modulus of nanotube, h is the thickness of nanotube. Since the representative surface is selected to instead of the representative volume, the thickness h appears here. As shown in Fig. 6, the trends of In-Plane stiffness Yh by the present study have some differences with the results by exponential CBR [4] and higher order CBR [7] even they all range from 180 to 235 Nm (graphite sheet state). In order to display this difference in trend, Fig. 7 shows that Young's modulus of SWCNTs is normalized by that of graphite sheet to compare with the results by the empirical tight-binding method [15]. It is observed that the present study is in better agreement with the tight-binding simulations [15] than exponential CBR [4] and higher order CBR [7] over a wide range of CNT diameter.

Conclusions

In summary, the present study has discovered that the mechanical phenomena of monolayer crystal films are governed by their inscribed surface, not atomic surface. Based on this congenital advantage of inscribed surface, a new extension of CBR, called inscribed CBR, is proposed to build a rigorous and accurate atomistic continuum theory. It straightly connects the continuum mechanics with monolayer crystal films at nanoscale. Applications of this theory to the graphite sheet and SWCNTs are validated by previously reported empirical studies.

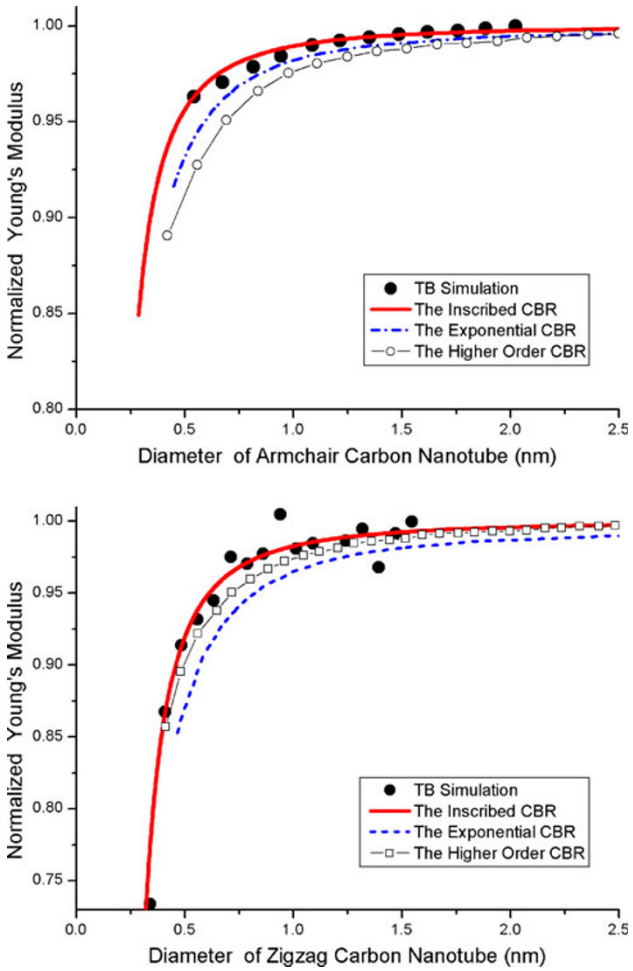

Fig. 7 Normalized Young's modulus versus diameter of nanotube

Acknowledgment This work was supported by Inha University.

References

1. M. Born, K. Huang, *Dynamical Theory of the Crystal Lattices* (Oxford University Press, Oxford, 1954)
2. E. Tadmor, M. Ortiz, R. Phillips, Philos. Mag. A **73**, 1529 (1996)
3. M. Arroyo, T. Belytschko, J. Mech. Phys. Solids **50**, 1941 (2002)
4. M. Arroyo, T. Belytschko, Phys. Rev. B **69**, 115415 (2004)
5. R. Sunyk, P. Steinmann, Int. J. Solids Struct. **40**, 6877 (2003)
6. X. Guo, J.B. Wang, H.W. Zhang, Int. J. Solids Struct. **43**, 1276 (2006)
7. J.B. Wang, X. Guo, H.W. Zhang, J.B. Liao, Phys. Rev. B **73**, 115428 (2006)
8. S. Lu, C.D. Cho, L. Song, Int. J. Mod. Phys. B **22**, 5881 (2008)
9. C.S.G. Cousins, J. Phys. C Solid State Phys. **11**, 4867 (1978)
10. E.B. Tadmor, G.S. Smith, N. Bemstein, E. Kaxiras, Phys. Rev. B **59**, 235 (1999)
11. P. Zhang, Y. Huang, P.H. Geubelle, P.A. Klein, K.C. Hwang, Int. J. Solids Struct. **39**, 3893 (2002)
12. J. Tersoff, Phys. Rev. B **37**, 6991 (1988)
13. D.W. Brenner, Phys. Rev. B **42**, 9458 (1990)
14. D.H. Robertson, D.W. Brenner, J.W. Mintmire, Phys. Rev. B **45**, 12592 (1992)
15. E. Hernándezl, C. Goze, P. Bernier, A. Rubio, Phys. Rev. Lett. **80**, 4502 (1998)